Effect of ceramic particles on precipitation in an Al-Mg-Si alloy with silicon excess during ageing

Gwenaëlle Meyruey[1,*], *Véronique* Massardier[1], and *Michel* Perez[1]

[1]Univ. Lyon, INSA Lyon, MATEIS – UMR CNRS 5510, Bât. Saint-Exupéry, 25 avenue J. Capelle, F-69621 Villeurbanne Cedex, France

Abstract. Providing a good balance between lightweight and high mechanical properties, the aluminum-based metal matrix composites (MMC) became an interesting alternative for specific industrial applications. However, considering an Al-Mg-Si alloy with a high silicon excess, the ceramic particles added as reinforcement can act on : i) the precipitation kinetics of the coherent and semi-coherent phases, ii) the precipitation sequence of the alloy and iii) the loss of mechanical strength from a peak-aged microstructure obtained by a T6 condition. In order to understand the influence of reinforcement on these aspects, the composite was characterized during isothermal ageing between 100°C and 350°C, allowing us to propose an experimental Isothermal Transformation Curve. Compared to the unreinforced alloy, heterogeneous precipitation of disordered semi-coherent phases occurs on dislocations and the precipitation kinetics were found to be accelerated in the composite leading to an acceleration of the loss of strength from the T6 state, due to the precipitation of the Type-C phase. A study performed on a deformed alloy, demonstrated that the most of the differences observed between the unreinforced alloy and the composite can be explained by the high dislocation density generated in the matrix of the composite due to the presence of ceramic particles. Finally, the JMAK approach turned out to be a powerful tool to model the decrease in mechanical strength occurring during isothermal treatments from T6 state.

1 Introduction

The aluminum-based metal matrix composites (MMC) have been developed for specific applications such as aerospace, aeronautic and automotive fields [1-2]. The addition of ceramic particles to Al-Mg-Si alloys is a successful method to achieve a good combination between lightweight, high mechanical properties at elevated temperatures and good conductivity properties.
In some cases, silicon can be in excess in Al-Mg-Si alloys, since it enhances the forming properties and the alloy's yield strength. In particular, the silicon excess increases the maximum mechanical strength reached after a T6 treatment (8 hours at 170 °C) [3-4].
However, both the addition of silicon excess and ceramic particles affect the precipitation sequence and its kinetics during artificial ageing. The study of the impact of these two factors on microstructural modifications during ageing has a particular interest for industrial applications since it can lead to changes of mechanical properties during the use of the materials.

Al-Mg-Si alloys are characterized by their structural hardening property attributed to the precipitation of the coherent needle-shaped β'' phase during ageing. In the literature, several studies proved that the peak in mechanical strength, achieved after the T6 treatment, is higher and reached earlier, with an increase in the silicon excess [5-7]. However, it is generally accompanied by an acceleration of the over-ageing, resulting in a sudden loss of mechanical strength beyond the peak. The precipitation sequence is also affected by the silicon excess since it is marked by the formation of new semi-coherent precipitates, besides the conventional quasi-binary semi-coherent β' phase, named Type-A, Type-B and Type-C, distinguished by their crystallographic properties as detailed in the literature [8-14].

A recent study [15], carried out on the effect of silicon excess in an unreinforced Al-Mg-Si alloy on the precipitation kinetics and microstructural evolutions during isothermal ageing, between 100°C and 350°C, highlighted that precipitation can be correlated to ThermoElectric Power (TEP) and Vickers hardness. The treatment conditions leading to high variations of TEP and hardness were characterized by Conventional and High-Resolution Transmission Electron Microscopy (C-TEM and HR-TEM) and provided the following precipitation sequence for the investigated alloy [15]:

$$\beta'' \rightarrow \beta'' + \text{Type-B} \rightarrow \text{Type-B/Type-A/Type-C } /\beta' + \text{Si particles}$$
$$\rightarrow \text{Type-A} + \text{Type-C} + \text{Si particles}$$

In this previous work, the β'' phase was found to be responsible for the maximum of strength as expected. Its precipitation was associated with an increase in hardness to its maximum value while, at the same time, the TEP decreased to its minimum value. Further ageing leads to

* Corresponding author: gwenaelle.meyruey@insa-lyon.fr

the precipitation of the Type-B phase followed by the Type-A and the Type-C. The beginning of the semi-coherent precipitation was correlated with a decrease in hardness and a TEP increase.
Using the TEP and hardness variations during ageing, combined with the microstructural characterization, an isothermal transformation curve (Time Temperature Precipitation diagrams) was proposed in the considered temperature range.
Finally, the loss of alloy's strength was followed by hardness measurements from the T6 state during isothermal ageing. In this work, the Johnson-Mehl-Avrami-Kolmogorov (JMAK) formalism was an efficient approach to predict the hardness decrease.

In MMC, the ceramic particles affect the alloy microstructure during ageing. Namely, they lead to : i) a decrease in the grain size [16], ii) the presence of interfaces and residual stresses [17-18], and iii) a high dislocation density generated during cooling from solutionising temperature [19–21]. The effect of reinforcing particles on precipitation in Al-Mg-Si alloys has been widely studied in the literature. Based on the results obtained by TEP, hardness measurements, and Differential Scanning Calorimetry (DSC) [19,22–25], the presence of reinforcement seems to accelerate the β'' precipitation and it is explained by the abovementioned microstructural modifications [8,23,25–27]. By means of the same experimental techniques, an acceleration of the semi-coherent β' precipitation has been observed as well [34-36,38-40]. In this case, the high dislocation density is considered to be responsible for this acceleration since it provides preferential nucleation sites for the heterogeneous precipitation.

In spite of the numerous studies carried out on the effect of the ceramic particles on the Al-Mg-Si alloy behaviour during thermal ageing, the prediction of this behaviour remains difficult. Namely, several parameters (volume fraction, morphology, size and nature of reinforcement [16,28–30], matrix composition [31]…) have to be considered for the analysis of the results. In addition, in presence of silicon excess in the matrix, the effects were not extensively studied.
Considering this context, the aim of this work is to clarify how the ceramic particles act on the precipitation kinetics, the microstructural and the strength evolutions during the thermal treatment of an Al-Mg-Si alloy with silicon excess.
To this end, the same alloy as that studied in [15] reinforced with 10 % of carbide particles was investigated. In order to compare the isothermal transformation curve of the unreinforced and reinforced alloy, both TEP and hardness measurements were performed throughout ageing treatments. C-TEM/HR-TEM was also used for microstructural characterization and identification of the precipitates responsible for the main TEP and hardness variations observed.
In a second part, the Johnson-Mehl-Avrami-Kolmogorov (JMAK) formalism was used to predict the loss of strength during isothermal ageing between 100°C and 350°C from a T6 state and compare to the unreinforced alloy behaviour.
Lastly, the effect of a high dislocation density in the composite due to the presence of reinforcement was isolated considering a deformed alloy wherein dislocations were artificially introduced. Following the same procedure than for the reinforced alloy, the deformed alloy was characterized and its behaviour was compared with that of the composite.

2 Materials and experimental procedure

2.1 Material

The composite investigated in this work is an Al-Mg-Si alloy with silicon excess and reinforced with 10 % of carbide particles added to the molten metal. As illustrated in Fig. 1, the carbide particles, irregularly shaped, have a size between 15 and 20 µm. The thermal dilatation coefficient is of the order of $6x10^{-6}$ K^{-1}. The chemical composition of the alloy is Al-0.9 wt.% Mg_2Si-0.7 wt.% Si with a content in Fe and Mn of between 0.1-0.3 wt.% and 0.5-0.7 wt.% respectively.

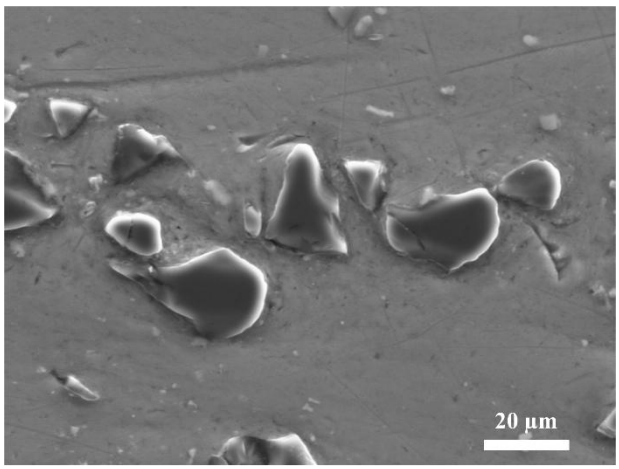

Fig. 1. SEM image of the reinforcement.

2.2 Thermal treatments

In order to follow the precipitation kinetics and the microstructural evolutions during ageing, the samples were, initially, solution treated for 1 hour at 540°C in a salt bath and water-quenched.

Artificial ageing was also carried out in salt bath at temperatures between 100°C to 350°C. The ageing was interrupted by water-quench after different treatment times to perform TEP or hardness measurements and microstructural characterization.

For the characterization of the loss of strength from a T6 state, a treatment of 8 hours at 170°C was made between homogenization and artificial ageing.

2.3 Experimental techniques

2.3.1 ThermoElectric Power (TEP)

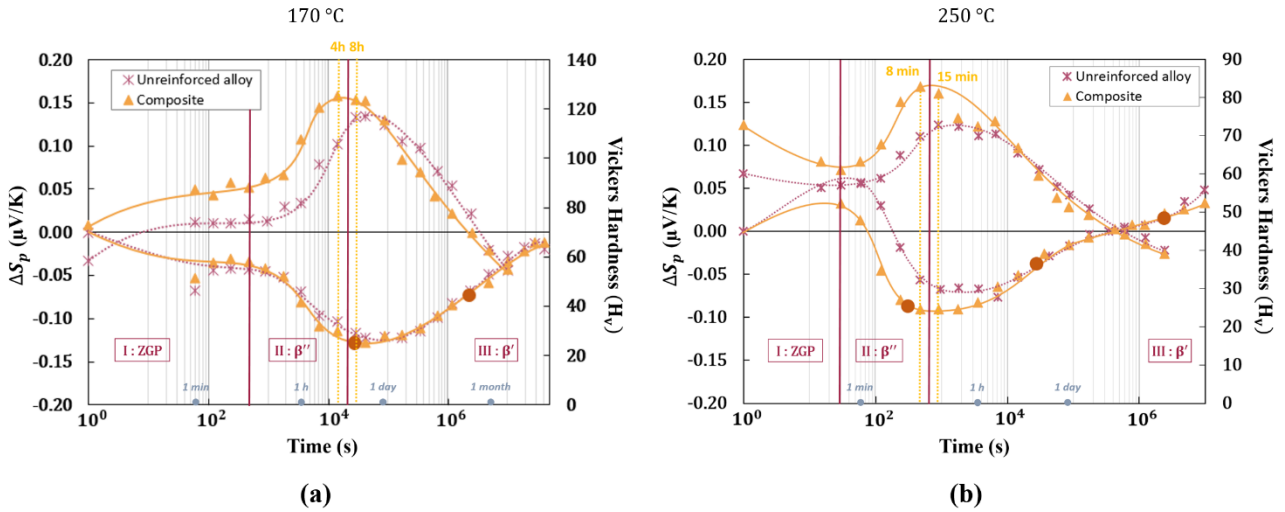

Fig. 2. Comparison of the hardness and TEP evolution of the unreinforced alloy and the composite during isothermal ageing at (a) 170°C and (b) 250°C.

This technique was used to follow, indirectly, the microstructural transformations occurring during heat treatment. The measured TEP variations, noted ($\Delta S_p(T,t)$), during ageing for a time t at temperature T are the result of two main contributions: one due to the alloying elements in solid solution ($\Delta S_{ss}(T,t)$) and one due to the intrinsic effect of precipitates ($\Delta S_{pre}(T,t)$).
In this work, the TEP measurements were performed at room temperature on samples 70 mm long, 5 mm wide and 1 mm thick.
More details on the technique and on the influence of the parameters of the microstructure on the TEP can be found in paper [15].
Based on previous work [27], it was considered that the reinforcement does not affect the TEP variations measured in the matrix.

2.3.2 Hardness

The hardness measurements were performed on samples 5 mm thick with an applied load of 1 kg on a BUEHLER Micromet 500 apparatus. As in the case of the TEP measurements, the hardness measurements were performed after different treatments times. The values, presented in this work, are averaged values of 10 measurements.

2.3.3 Transmission Electron Microscopy (TEM)

The microstructural characterization by TEM was used to identify the phases responsible for the TEP and hardness variations observed during ageing treatments. Selecting the appropriate ageing states, the samples were first characterized by Conventional-TEM (C-TEM) in order to determine the morphology and the average size of precipitates. These observations were performed on a Jeol 2100 microscope equipped with a CCD camera Gatan Orius SC1000. Then, for more precise information, such as the crystallography and nature of precipitates the samples were characterized by High Resolution - TEM (HR-TEM). In this case, the observations were performed on a field-emission gun Jeol 2010 microscope.

The composite thin foils were mechanically thinned from the bulk sample after ageing treatment, and thinned by ion beam.

The precipitates were observed along a $<100>_{Al}$-zone axis. The identification of the precipitates was based on the numerical fast-Fourier transforms of the images obtained with the CCD camera.

3 Results

3.1 Characterization of the precipitation from the supersaturated solid solution state

3.1.1 Study of the TEP and hardness kinetics during isothermal ageing

TEP and hardness measurements were carried out during isothermal ageing and compared during a treatment at 170 °C and 250 °C after quench from the solid solution state for both the unreinforced alloy and the composite. Fig.2 illustrates the perfect correlation between the TEP and hardness kinetics; the microstructural modifications responsible for the decrease in TEP gives rise to a hardness increase and conversely, a hardness decrease corresponds to a TEP increase.

Due to their high sensitivity to microstructural modifications, these techniques reflects the complex transformations taking place during thermal treatment. In Fig.2, three domains can be defined:

- Domain I : TEP/hardness variations are related to the Guinier-Preston zones (GPZ). At low temperatures, the GPZ can precipitate and generate an hardness increase (TEP decrease) as observed in fig.2.(a) for an ageing at 170 °C. At higher temperatures, the GPZ already created during the quench after solution treatment are dissolved resulting in a hardness decrease (TEP increase) illustrated in Fig.2.(b).
- Domain II : marked by the hardness increase until the maximum value (respectively, TEP decrease until its

minimum). This significant variation, seen in Fig.2(a) and (b), can be attributed to the precipitation of the hardening phase, β''. The maximal value reached is higher at 170°C because this temperature corresponds to the conditions giving the finer microstructure and the higher density of β''.

- Domain III : defined by a sharp hardness decrease (TEP increase) corresponding to the precipitation of the semi-coherent phases.

Considering the domain I, no effect of ceramic particles can be deduced from the TEP/hardness measurements. The magnitude of the hardness/TEP variations and the kinetics are similar for the alloy and the composite, indicating that the density of GPZ formed could be more or less identical. In the domain II, the reinforcement leads to an acceleration of the kinetics and a higher hardness peak. In the domain III, the composite exhibits a faster loss of strength beyond the peak, meaning that the precipitation of semi-coherent phase would begin sooner.

In order to understand the microstructural transformation responsible for the difference of behaviour, C-TEM and HR-TEM characterization was used for specific ageing conditions: 8 hours and 1 month at 170°C, 6 minutes, 8 hours and 1 month at 250°C. These treatments can be located on the hardness/TEP kinetics of Fig. 2 thanks to the orange points

3.1.2 TEM characterization of the microstructure evolution

TEM characterization in peak-aged conditions highlighted that the homogeneous precipitation of β'' and the heterogeneous precipitation of a semi-coherent and disordered phase on dislocations occur simultaneously (Fig.3.) in the early stages of ageing of the reinforced alloy, while it has not been observed in the unreinforced alloy. As illustrated in Fig.4., after the peak hardness the loss of strength obtained after 1 month at 170°C and 8 hours at 250°C is mainly due to the precipitation of the Type-C phase, even if the microstructure contains also Type-B and β' phases. In over-aged conditions (1 month at 250°C), the microstructure consists in a mixture of Type-C and Type-A precipitates with the Type-A precipitate as main phase.

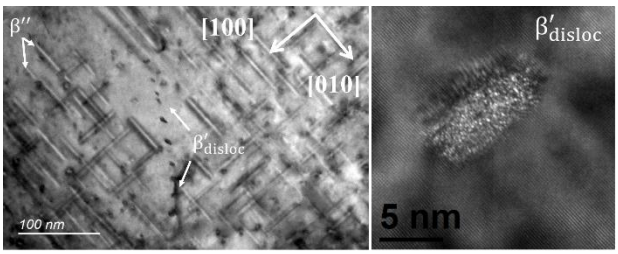

(a) (b)

Fig. 3. (a) C-TEM and (b) HR-TEM micrographs of disordered β'_{disloc} phase observed after 6 minutes at 250°C in the

Based on the precipitates identified in the ageing states characterized by TEM, the following precipitation sequence could be proposed:

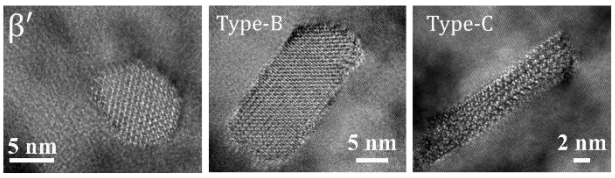

(a) (b) (c)

Fig.4. TEM micrographs of semi-coherent phases responsible for the loss of strength in the composite during isothermal ageing

$$\text{Solid Solution} \rightarrow \text{ZGP} \rightarrow \mathbf{\beta''} + \beta'_{disloc} + \beta' \rightarrow \text{Type-B} + \beta' + \mathbf{\text{Type-C}} + \text{Type-A} \rightarrow \mathbf{\text{Type-A}} + \text{Type-C}$$

3.1.3 Isothermal Transformation Curve

The isothermal transformation curves for the unreinforced and reinforced material were built from the TEP kinetics obtained at different temperatures. They present two lines: the first line indicating the time corresponding to the beginning of the coherent precipitation (β'') and the second corresponding to the beginning of the semi-coherent precipitation. The method used to obtain the Isothermal Transformation Curve is described in paper [15]. Fig.5. reflects the acceleration of the coherent/semi-coherent precipitation in the composite and a decrease in the stability domains of the β'' phase and of the semi-coherent phases.

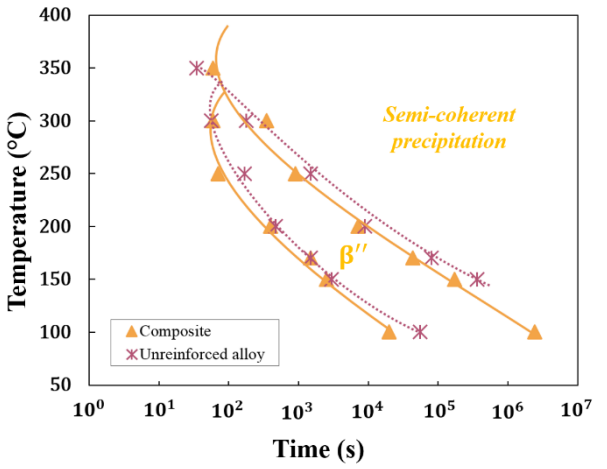

Fig.5. Comparison of the isothermal transformation curves of the unreinforced alloy and the composite.

3.2 Effect of reinforcement on the loss of strength during ageing from a T6 state

Following the same procedure as for the unreinforced alloy (described in paper [15]), the hardness *H(t)* of the T6-treated composite was measured during isothermal ageing for 100°C ≤ *T* ≤ 350°C. Similarly to the alloy behaviour detailed in [15], the hardness curves for all ageing treatments performed at *T* are stackable for an activation energy *Q* of 120 kJ/mol. The good superposition is due to the thermal activation of the phenomena leading to the hardness decrease and can be obtained thanks to a time-temperature equivalence based

on an Arrhenius law. Afterwards, the hardness curves, due to their sigmoidal shape, were fitted by an isothermal Johnson-Mehl-Avrami-Kolomogorov (JMAK) approach defined by the following relation :

$$Y(T,t) = 1 - \exp(-(kt)^n) \quad (1)$$

$$\text{With } k = k_0 . \exp\left(-\frac{Q}{RT}\right) \quad (2)$$

where $Y(T,t) = \frac{H(t)-H_{max}}{H_{min}-H_{max}}$ is the transformed fraction (0<Y<1) with H_{min} the minimum hardness value and H_{max} the maximum hardness value (T6 state), n the Avrami exponent, k_0 a constant and R the gas constant. After having determined the parameters (n, k_0 and Q) of this law for the composite material (Table 1), this approach allowed the proper description of the strength evolution and the mechanical property prediction for extremely long-term ageing as illustrated in Fig.6(a).

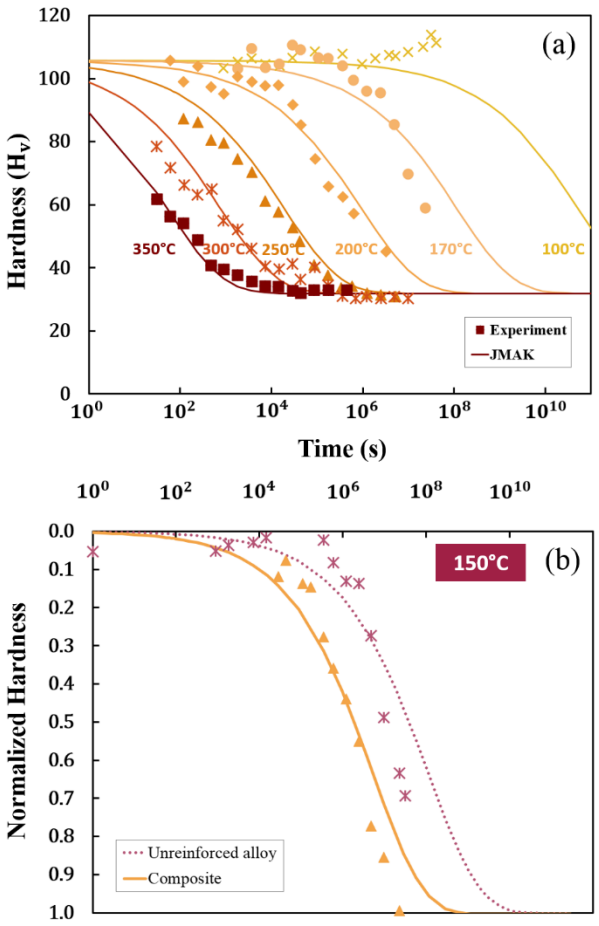

Fig.6. (a) Hardness decrease measured from a T6 state and fitted with JMAK law for different isothermal treatments of the composite material between 100°C and 350°C. (b) Comparison of the normalized hardness evolution of the alloy and of the composite for an ageing at 150°C.

Considering the parameters of Table 1, the normalized hardness kinetics of the unreinforced and reinforced alloys were plotted from the experimental data at 150 °C and modeled with the JMAK approach (Fig.6(b)). Fig.6(b) highlights the acceleration of the loss of strength due to the reinforcement added in the matrix. This result is correlated to the premature precipitation of semi-coherent phases in the composite observed by TEM characterization. The difference of behaviour is reflected in the lower activation energy value in the case of the composite. By comparison, the activation energies for the diffusion of magnesium and silicon in aluminum are, respectively, 130 kJ/mol and 124 kJ/mol. The activation energy of 160 kJ/mol estimated for the alloy suggests that the loss of strength could be governed by nucleation of semi-coherent phases and diffusion of the alloying elements. However, since the activation energy of the composite is very close to that for the diffusion of Mg and Si, it indicates that the strength loss is mainly controlled by the diffusion of these two elements. Furthermore, this phenomenon is enhanced in the matrix of the composite due its high dislocation density. The presence of dislocations results in: (i) preferential diffusion paths, accelerating both the coherent and semi-coherent precipitation and the coarsening phenomena, (ii) heterogeneous nucleation sites, promoting the nucleation of the semi-coherent phases. In order to validate the predominant role of dislocations in the differences observed between the alloy and the composite in this study, a deformed alloy (with dislocations artificially introduced by cold-rolling) was characterized.

Table 1. Summary of the JMAK parameters for the alloy (cold-rolled and undeformed) and the composite.

	Alloy	Deformed alloy	Composite
Q (kJ/mol)	160 (+/- 5)	135 (+/- 5)	120 (+/- 15)
n	0.35	0.34	0.38
k_0 (s^{-1})	5.25 x 10^{11}	2.5 x 10^9	9.91 x 10^7

3.3 Effect of the presence of dislocations in the alloy on microstructural evolutions during ageing

Due to the significant difference in the thermal expansion coefficients between the alloy and the ceramic particles, a high dislocation density is generated in the matrix of the composite material during cooling from the solutionizing temperature. With the aim of demonstrating that dislocations are mainly responsible for the differences observed between the alloy and the composite in this work, a deformed alloy was studied. To this end, an alloy sample was cold-rolled with a reduction ratio of 2.4 % after homogeneisation and water-quench.

The deformed alloy underwent an isothermal ageing at 170 °C interrupted to perform hardness measurements and the results were compared with the undeformed alloy and the composite. As shown in Fig.7, the deformed alloy exhibits the same kinetics as that of the composite and reaches the same maximum value.

From TEM observations of the deformed alloy aged 8 hours at 250 °C, it was established that the Type-C is the prevailing phase. As revealed for the composite, the Type-C is responsible for the loss of strength in the cold-rolled alloy wherein dislocations were introduced, while it was the Type-A for the undeformed alloy. This result is in good agreement with a previous study showing that dislocations promote the Type-C precipitates [32].

Starting from the T6 state, the hardness decrease during isothermal ageing can also be predicted with the JMAK law described above determining the JMAK parameters (given in Table 2). An increase in the dislocation density of the alloy leads to Q and k_0 values closer to those of the composite. These results confirm that the acceleration of the loss of strength in the composite mainly comes from the dislocations. Fig.8(b) compares the hardness decrease predicted by the JMAK for the undeformed alloy, the cold-rolled alloy and the composite during an ageing at 250 °C. The deformed alloy shows the same acceleration of the hardness decrease in the early stages of the treatment but, in overaged conditions, the curve reaches the same final value as for the undeformed alloy. This observation suggests that, recovery or recrystallization took place in the deformed alloy for long ageing times, and that other elements contributes to the hardening of composite in over-aged conditions.

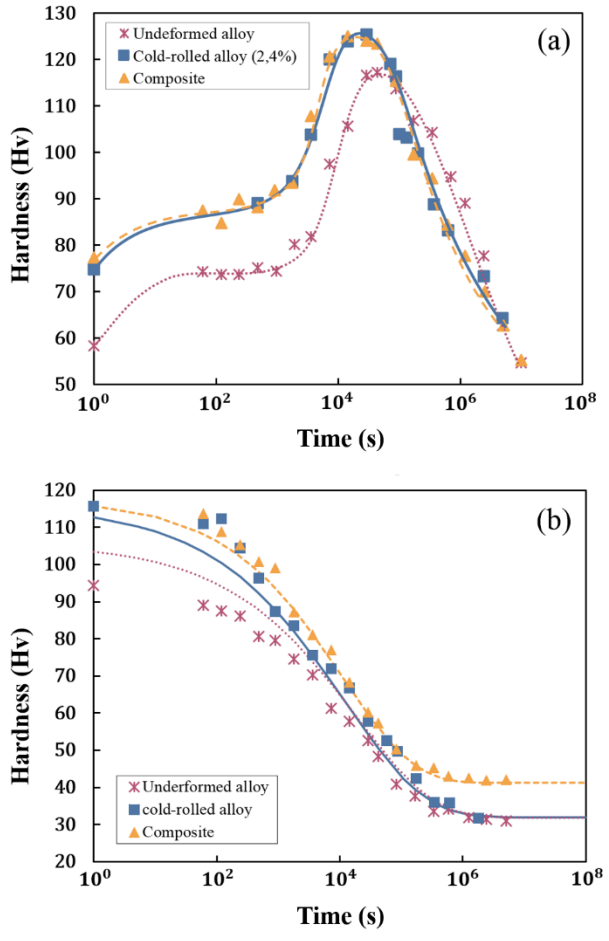

Fig.8. (a) Comparison of the hardness kinetics during ageing at 170 °C for the unreinforced alloy, deformed alloys and the composite. (b) Comparison of the decrease in hardness from the T6 state during ageing at 250°C predicted by the JMAK law for the undeformed alloy, the cold-rolled alloy and the composite.

4 Conclusion

The aim of this study was to understand how the ceramic particles act on the matrix microstructure during isothermal ageing and the consequences on mechanical properties considering an Al-Mg-Si alloy with silicon excess.

The reinforcement accelerates the precipitation of the coherent and semi-coherent phase leading to an acceleration of the loss of strength from the T6 state. The microstructure is more heterogeneous even in the early stages of ageing since dislocations induced by the particles lead to premature precipitation of semi-coherent phase and disordered precipitates. Studying a cold-rolled alloy, the major role of dislocations in the difference of behaviour observed between the alloy and the matrix has been confirmed. It was also shown that dislocations promote the precipitation of the Type-C phase, which is responsible for the loss of strength in the composite and deformed alloy while this phase was barely observed in the undeformed alloy.

The JMAK model is a powerful tool to predict the hardness decrease from the T6 state during isothermal ageing and considering the appropriate JMAK parameters defined in this study. This approach links the acceleration of the hardness decrease in the composite to a lower activation energy of the phenomenon explained by the higher dislocation density acting as diffusion path for alloying elements and promoting the nucleation of semi-coherent phase. The same approach applied to deformed alloy confirms the role of dislocation in the activation energy decrease and suggests that the dislocations are the main factor responsible for the acceleration of the loss in composite strength as long as the recovery phenomena do not come into play.

Acknowledgments

We would like to thank the Clym (Consortium Lyonnais de Microscopie) for access to the 2010F and 2100 microscope and to N. Blanchard for his kind assistance with the Conventional TEM observations.

References

1. S. Mazumdar, *State of composites industry*, Composite Manufacturing, 1–6 (2016)
2. L. Berreur, B. DeMaillard, S. Nosperger, *L'industrie française des matériaux composites*, Nodal Consultant (2002)
3. K. Fukui, M. Takeda, T. Endo, Journal Japan Inst Met, **46**, 880-884 (2006)
4. A.K. Gupta, D.J. Lloyd, S.A. Court, Mater Sci Eng, **316**, 11–17 (2001)
5. J.P. Lynch, L.M. Brown, M.H. Jacobs, Acta Metall, **30**, 1389-1395 (1982)
6. Y. Ohmori, L.C. Doan, K. Nakai, Mater Trans, **43**, 246-255 (2002)
7. L.C. Doan, K. Nakai, Y. Matsuura, S. Kobayashi, Y. Ohmori, Mater Trans, **43**, 1371–1380 (2002)
8. K. Matsuda, S. Tada, S. Ikeno, T. Sato, A. Kamio,

Scr Metall Mater, **32**, 1175–1180 (1995) (1999)

9. K. Matsuda, T. Naoi, K. Fujii, Y. Uetani, Mater Sci Eng A, **262**, 232–237 (1999)
10. K. Matsuda, Y. Sakaguchi, Y. Mitaya, Y. Uetani, T. Sato, A. Kamio, et al., Mater Sci, **35**, 179–189 (2000)
11. K. Matsuda, S. Ikeno, T. Sato, A. Kamio, Acta Metall, **34**, 1797–1802 (1996)
12. P. Derlet, S. Andersen, C. Marioara, A. Froseth, J Phys Condens Matter, **14**, 4011–4024 (2002)
13. A. Froseth, S. Andersen, C. Marioara, P. Derlet, R. Hoier, *Solving the Structure of the Phases in the Al-Mg-Si Alloy System with the Help of Ab Initio Modelling*, MRS Online Proceeding Libr Arch, (2002)
14. A. Froseth, R. Hoier, P. Derlet, S. Andersen, C. Marioara, Phys Rev B, **67**, 1-11 (2003)
15. G. Meyruey, V. Massardier, W. Lefebvre, M. Perez, Mater Sci Eng A, **27,** 92-105 (2018)
16. F. Humphreys, H. Lilholt, O. Pederson, *Deformation and annealing mechanisms in discontinuously reinforced metal-matrix*, Proc 9th Riso Int Symp Mech Phys Behav Met Ceram Compos, 51–74 (1988)
17. Z.M. Sun, J.B. Li, Z.G. Wang, W.J. Li, Acta Met Mater, 40, 2961–2966 (1992)
18. M. Suery, C. Teodosiu, L.F. Menezes, Mater Sci Eng, **167**, 97–105 (1993)
19. S. Suresh, T. Christman, Scr Metall, **23**, 1599–1602 (1989)
20. R.J. Arsenault, L. Wang, C.R. Feng, Acta Metall Mater, **39**, 47–57 (1991)
21. M. Vogelsang, R.J. Arsenault, R.M. Fisher, Metall Trans A, **17**, 379–389 (1986)
22. S. Abis, G. Donzelli, J Mater Sci Lett, **7**, 51–52 (1988)
23. T.G. Nieh, R.F. Karlak. Scr Metall, **8**, 25–28 (1984).
24. M. Hadianfard, Y. Mai, J. Healy, J Mater, **28**, 3665–3669 (1993)
25. M. Gupta, M. Surappa, Mater Res Bull, **30**, 1023–1030 (1995)
26. J.M. Papazian, Metall Trans A, **19**, 2945–2953 (1988).
27. D. Dafir, G. Guichon, R. Borrelly, S. Cardinal, P.F. Gobin, P. Merle. Mater Sci Eng A, **144**, 311–318 (1991)
28. N.K. Sharma, R.K. Misra, S. Sharma, Ceram Int, **43**, 513–522 (2017)
29. N. Ramakrishnan, Acta Mater, **44**, 69–77 (1996).
30. G. Meijer, F. Ellyin, Z. Xia, Compos Part B Eng, **31**, 29–37 (2000)
31. V. Massardier, P. Merle, Mater Sci Eng A, **249**, 109–120 (1998)
32. K. Matsuda, S. Shimizu, H. Gamada, Y. Uetani, F. Shinagawa, S. Ikeno, J Soc Mat Sci, 48, 10–15